Cerebral Cortex April 2008;18:763–770
doi:10.1093/cercor/bhm117
Advance Access publication July 17, 2007

Hyperconnectivity of Local Neocortical Microcircuitry Induced by Prenatal Exposure to Valproic Acid

Tania Rinaldi[1], Gilad Silberberg[1,2] and Henry Markram[1]

[1]Laboratory of Neural Microcircuitry, Brain Mind Institute, Ecole Polytechnique Fédérale de Lausanne (EPFL), Lausanne 1015, Switzerland and [2]Nobel Institute for Neurophysiology, Department of Neuroscience, Karolinska Institute, Stockholm, Sweden

Exposure to valproic acid (VPA) during embryogenesis can cause several teratogenic effects, including developmental delays and in particular autism in humans if exposure occurs during the third week of gestation. We examined the postnatal effects of embryonic exposure to VPA on microcircuit properties of juvenile rat neocortex using in vitro electrophysiology. We found that a single prenatal injection of VPA on embryonic day 11.5 causes a significant enhancement of the local recurrent connectivity formed by neocortical pyramidal neurons. The study of the biophysical properties of these connections revealed weaker excitatory synaptic responses. A marked decrease of the intrinsic excitability of pyramidal neurons was also observed. Furthermore, we demonstrate a diminished number of putative synaptic contacts in connection between layer 5 pyramidal neurons. Local hyperconnectivity may render cortical modules more sensitive to stimulation and once activated, more autonomous, isolated, and more difficult to command. This could underlie some of the core symptoms observed in humans prenatally exposed to valproic acid.

Keywords: autism, connectivity, in vitro electrophysiology, juvenile rat, somatosensory cortex, synaptic strength

Introduction

Many neurological disorders are believed to have a teratogenic origin, with initial alterations starting before the brain is fully developed. Evidence for cortical alterations in these disorders have been demonstrated, like minicolumnar abnormalities (Casanova et al. 2002) or perceptual processing abnormalities (see Rubenstein and Merzenich 2003) in autism. The study of these disorders can therefore be a valuable tool, beside the understanding and treatment of the disorder itself, to understand the crucial equilibrium of the healthy brain. Valproic acid (VPA) is an antiepileptic drug that is known to be strongly teratogenic. Indeed, VPA has been shown by numerous case and epidemiological studies (Christianson et al. 1994; Williams and Hersh 1997; Moore et al. 2000; Williams et al. 2001; Rasalam et al. 2005) to greatly increase the risk for developmental delays and autism in the exposed embryo. Women under VPA treatment do typically take this drug throughout the pregnancy, but the timing for the teratogenic effect of VPA increasing the risk for autism is shown to be around the time of neural tube closure (E20–24) (Rodier et al. 1997; Arndt et al. 2005).

Previous studies explored the results of prenatal VPA exposure during the equivalent embryonic stage in rats and found similar gross abnormalities to those in autism, such as diminished number of cerebellar Purkinje cells and signs of brainstem damage (Ingram et al. 2000; Sobaniec-Lotowska 2001). Behavioral studies further showed that a number of autistic core symptoms, such as impairments in social interactions and higher sensitivity to sensory stimulation, are also present in VPA-treated rats (Schneider and Przewlocki 2005; Markram et al. 2007). How prenatal VPA exposure affects the brain in terms of the functioning of synapses, neurons, and microcircuit in general is however unknown.

In this study we therefore compared the basic properties of the neocortical microcircuit in control and VPA-treated rats. Our results show striking differences in the microcircuit connectivity as well as intrinsic properties of neocortical pyramidal neurons. These differences might underlie some of the core symptoms observed in children exposed to VPA.

Materials and Methods

The VPA Rat Model of Autism

All experimental procedures were carried out according to the Swiss federation rules for animal experiments. Wistar Han rats (Charles River Laboratories, L'Arbresle, France) were mated, with pregnancy determined by the presence of a vaginal plug on embryonic day 0 (E0). The sodium salt of valproic acid (NaVPA, Sigma-Aldrich, Lausanne, Switzerland) was dissolved in 0.9% saline for a concentration of 150 mg/mL, pH 7.3. The dosing volume was 3.3 mL/kg; the dosage was adjusted according to the body weight of the pregnant rat on the day of injection. Treated rats received a single intraperitonal injection of 500 mg/kg NaVPA on gestational day 11.5, and control rats were untreated (Ingram et al. 2000). Delivery of this dose to rats during embryogenesis has been shown to result in maximum levels of total VPA in maternal plasma in less than 1 h, with a mean plasma elimination half-life of 2.3 h (Binkerd et al. 1988). We verified that infants of saline-injected rats did not show any difference in behavior compared with control untreated rats (data not shown). Unchanged litter size, pup body weight, and general health of the mothers and pups were indications of normal rearing conditions for treated rats. Rats were housed individually and were allowed to raise their own litters.

Acute Slice Preparation

Offspring (P12 to P16, cf. age distribution in Supplementary Table 1) were rapidly decapitated without anesthesia, and sagittal neocortical slices (300 μm thick) were sectioned on a vibratome (HR2, Sigmann Elektronik, Heidelberg, Germany) in iced artificial cerebral spinal fluid (ACSF). Optimal slices, with apical dendrites of cells running parallel to the slice surface, were selected for recording. They were incubated for 30 min at 35 °C and then at room temperature until transferred to the recording chamber (room temperature or 34 °C). The ACSF contained (mM) 125 NaCl, 2.5 KCl, 25 glucose, 25 $NaHCO_3$, 1.25 NaH_2PO_4, 2 $CaCl_2$, and 1 $MgCl_2$. Neurons in primary somatosensory cortex were identified using IR-DIC microscopy, with an upright microscope (Olympus BX51WI, fitted with a 60×/0.90 W objective, Olympus, Switzerland). Recorded neurons were selected up to 70 μm below the surface of the slice.

Electrophysiological Recording

Simultaneous whole-cell recordings from clusters of up to 7 neurons (pipette resistance 4–10 MΩ) were made and signals were amplified using Axopatch 200B amplifiers (Axon Instruments, Molecular Devices, Union City, CA). Neurons were submitted to different stimulation

protocols. Voltages (in current-clamp mode) or current (in voltage-clamp mode) were recorded with pipettes containing (mM) 110 potassium gluconate, 10 KCl, 4 ATP-Mg, 10 phosphocreatine, 0.3 GTP, 10 HEPES, and 0.5% biocytin (pH 7.3, 270–300 mOsm). In voltage-clamp experiments at +10 mV for measurement of GABA receptor–mediated currents, 10 μM QX-314 was added to the intracellular solution. Membrane potentials were not corrected for the junction potentials between pipette and bath solution (~10 mV). Thick-tufted pyramidal cells (PCs) were unambiguously identified by their soma shape and apical dendrite, as confirmed with histological identification of stained patched neurons.

Connectivity

Direct synaptic connections were examined by eliciting short regular trains (8 pulses) of precisely timed action potentials (APs) at 30-Hz frequencies followed by a recovery test response 500 ms later. The average synaptic response to the stimulation protocol allows the extraction of the basic parameters of the synaptic connection with a model of dynamic synaptic transmission (*A*, the absolute strength of the connection; *Pr*, equivalent to the probability of release; *D*, the time constant to recover from depression) (Tsodyks and Markram 1997).

For the observation of disynaptic connectivity, neighboring thick-tufted layer 5 PCs were recorded and stimulated with high-frequency regular AP trains (15 APs at 70 Hz). When PCs were connected via an intermediate interneuron, inhibitory responses were observed on neighboring PCs.

Intrinsic Neuronal Properties

During whole-cell current-clamp recordings, PCs were submitted to a set of stimulation protocols designed to capture their key active and passive electrical properties, as described by Le Be et al. (2006). In short, recordings were sampled at intervals of 10–400 μs using Igor Pro (Wavemetrics, Lake Oswego, OR), digitized by an ITC-18 interface (Instrutech, Great neck, NY), and stored for off-line analysis. For the study of the current–frequency (IF) relationship, current injections of amplitudes ranging from the current needed to reach AP threshold (I_{thresh}) to 4 times that current ($4 \times I_{thresh}$) were used; the points of the IF relationship were therefore in the linear range. The slope of the IF relationship was then defined as the slope of the linear regression fitting these points.

Multielectrode Array Stimulation

Multisite extracellular stimulations were performed using a multielectrode array (MEA) made of 60 3D tip-shaped platinum electrodes (electrode basis: 40 × 40 μm, electrode height: 50–70 μm, electrode interspace: 200 μm; Ayanda Biosystems, Ecole Polytechnique Fédérale de Lausanne, Lausanne, Switzerland). Acute brain slices were mounted with a solution of nitrocellulose (0.14 mg/mL in ethanol and 1% methanol). In order to increase the adherence of the slice to the MEA surface, the slice was cut to a width of 5–7 mm before mounting. The stimulations were made of 1-ms-long biphasic pulses of varying amplitude (0.1–2 V) and frequency. Neuronal responses were recorded in whole-cell patched layer 5 and layer 2/3 PCs. For the study of neuronal response with minimal network stimulation, a single MEA electrode was stimulated (minimal responses corresponded to single pulse stimulation of 0.7 V/1 ms), and currents were recorded in voltage-clamped layer 2/3 PCs (holding voltage of –80, –70, –60, –50, and –40 mV). Synaptic conductances could then be calculated according to the method described by Borg-Graham et al. (1996). The responses were integrated over a time window of 200 ms following stimulation. The normalization of the stimulation amplitude was based on the post-synaptic response in the current-clamped cells at resting potential to single pulse stimulation of each individual MEA electrodes: the normalized stimulation amplitude "10" corresponded to a response of 5 mV. The normalized stimulation amplitude was then linearly scaled; for example, the normalized stimulation amplitude 1 corresponded to stimulation amplitude of 0.1 times the stimulation amplitude needed for each electrode to evoke a response of 5 mV, the normalized stimulation amplitude 20 corresponds to twice that value. For the study of strong network stimulation, the 16 MEA electrodes giving rise to the strongest responses in the patched neurons were simultaneously stimulated with a Poisson train (50 Hz, 300 ms) at increasing stimulation amplitude (from 0.1 to 2 V, with increments of 0.1 V and 10-s interval between each stimulation). The responses to these stimulations were recorded in layer 5 PCs current clamped at –70 mV (as these cells are too big to be reliably voltage clamped) or in layer 2/3 PCs filled with QX-314 voltage clamped at –80, –57, and +10 mV (to get the contribution of global, excitatory, or inhibitory components, respectively). The responses were integrated over a time window of 5 s starting at the end of the MEA stimulation. Ninety-five percent of the response to MEA stimulation was blocked following bath application of synaptic blockers (40 μM D-APV, 10 μM CNQX, and 20 μM bicuculline), indicating that the response was synaptically mediated (Supplementary Fig. 2*B*).

Histological Procedures and Quantitative Morphological Analysis

After recording, slices were processed as described by Markram et al. (1997). The 3D neuron models were reconstructed using Neurolucida system (MicroBrightField Inc., Magdeburg, Germany) and a bright-field microscope (fitted with a 40×/0.75 W, a 60×/0.90 W, or a 100×/1.30 W objective, Olympus, Switzerland). The following parameters were analyzed: 1) Axonal Sholl intersection (ASI) and dendritic Sholl intersection (DSI), 2) soma diameter, 3) bouton, and 4) spine densities. The Sholl intersections are counted as the number of intersections the processes make at the given distance from the soma. Furthermore, the number of potential synaptic contacts between connected cells was determined by counting the number of times a bouton of the pre-synaptic axon was touching the postsynaptic dendrite.

Cell Counting

The counting of layer 5 PCs of the somatosensory cortex was based on IR pictures taken from a given volume of the acute slices (180 × 180 × 30 μm, stack of 15 pictures, 2-μm z-distance between starting 10 μm below the surface of the slice). The PCs were recognized by their characteristic apical dendrites, soma shape, and size and then counted.

TUNEL Staining

DNA fragmentation, a hallmark of apoptosis, was detected by terminal deoxynucleotidyl transferase–mediated dUTP nick-end labeling (TUNEL) assay as previously described (Brionne et al. 2003). In all, 20–30 sagittal cryosections (8 μm) per brain were fixed in 4% paraformaldehyde for 20 min, permeabilized with 0.1% Triton X-100, acetylated for 10 min, dehydrated through ethanol series, incubated with digoxygenin-labeled dUTP and deoxynucleotidyl transferase (Roche, Basel, Switzerland) at 37 °C for 1 h, and labeled with FITC-conjugated anti-digoxygenin antibody (Roche). TUNEL-positive cells were viewed and counted by fluorescence microscopy. The brains from 2 control and 2 treated rats were used for this analysis.

Statistical Analysis

For comparison of frequencies (i.e., connection probabilities in our case), we used 2-sided χ^2 test. For comparison of means, we used the 2-sample Student's *t*-tests (log-transformation was first applied to skewed distribution of the synaptic parameter *A*). We compared cumulative distributions of axonal and dendritic tree measures nonparametrically using the 2-sample Kolmogorov–Smirnoff test. Statistics reported in the text and figures represent the mean ± standard error of mean (SEM). For the connection probabilities, the error bars express the standard error estimate based on the formula SEM = sqrt ($P(1 - P)/(n - 1)$), where P is the probability. This enables the reader to visualize the uncertainty given the proportion P and the denominator n. The number n represents the number of cells for Figures 2, 3, and 4 and the number of pairs for Figure 1. The number of clusters, rats, and litters used for each experiment are detailed in Supplementary Table 2.

Results

Increased Probability of Local Connections

We examined the effect of a single VPA injection into pregnant rats (intraperitonal injection on gestational day 11.5, 500 mg/kg NaVPA) (Ingram et al. 2000) on the microcircuitry of the offspring neocortex 2 weeks after birth. This timing of prenatal

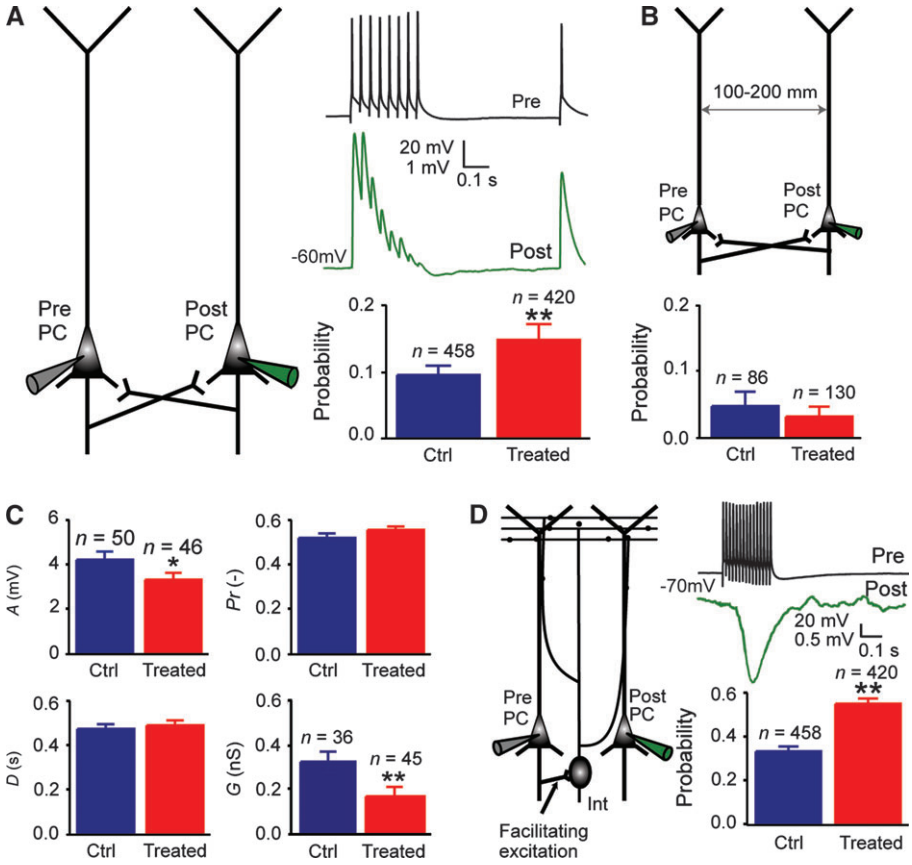

Figure 1. Hyperconnectivity of local microcircuitry. (*A*) Increased probability of direct connection between layer 5 PCs in a cluster. (*B*) No hyperconnectivity at longer distances. (*C*) Parameters describing the functional synaptic transmission dynamic extracted from fitting the connections with the Tsodyks–Markram model: *A*, the absolute synaptic strength equal to the maximal possible synaptic output; *Pr*, the utilization of synaptic efficacy equivalent to the probability of release; *D*, the time constant of synaptic depression. Weakened synapses were consistent with the decreased synaptic conductances (*G*) evoked by minimal extracellular stimulation. (*D*) Increased number of disynaptic connections between thick-tufted layer 5 PCs (via interneuron [Int] between the 2 PCs). Data show mean ± SEM (*$P < 0.05$; **$P < 0.01$; probabilities were compared using the 2-sided χ^2 test, means were compared using the 2-sample Student's *t*-test).

rat exposure corresponds to the human developmental period most vulnerable to VPA teratogenic insults linked to autism (Rodier et al. 1997). We prepared slices of the primary somatosensory cortex for electrophysiological in vitro studies in a standard manner and used infrared differential interference contrast microscopy (IR-DIC) to perform multineuron patch-clamp recordings from visually identified PCs. This approach allows direct and detailed measurement of the microcircuit properties.

We found that the number of direct connections established between layer 5 thick-tufted PCs was increased by more than 50% (0.10 ± 0.01, $n = 458$ pairs for control; 0.16 ± 0.02, $n = 420$ pairs for treated; $P < 0.01$; Fig. 1*A*). This hyperconnectivity was only found for close neighboring neurons within the dimensions of a neocortical minicolumn (~50-μm somatic distance; Buxhoeveden and Casanova 2002), because the probability of connection was unchanged for pairs of PCs 100–200 μm apart (0.05 ± 0.02, $n = 86$ pairs for control; 0.03 ± 0.02, $n = 130$ pairs for treated; $P > 0.05$; Fig. 1*B*).

We further examined the biophysical properties of these synaptic connections by fitting them with a model of dynamic synaptic transmission (Tsodyks and Markram 1997). This model proposes a set of 3 parameters for quantifying transmission dynamic: *A*, the absolute synaptic efficacy, is the maximum strength that can be given by a connection; *Pr*, the utilization of synaptic efficacy, can be associated with the probability of release; and *D*, the time constant to recover from depression (Markram et al. 1998). In slices from VPA-treated rats, we found that the maximal possible synaptic output was significantly weaker (*A*: 4.2 ± 0.4 mV, $n = 50$ connections for control; 3.3 ± 0.3 mV, $n = 46$ connections for treated; $P < 0.05$) while neither the probability of neurotransmitter release (*Pr*) nor the time constant of synaptic depression (*D*) were significantly affected (Fig. 1*C*). Next, we measured the postsynaptic conductances produced by minimal extracellular stimulation. The results also revealed weaker excitatory synaptic responses in VPA-treated rats (0.32 ± 0.05 nS, $n = 36$ neurons for control; 0.16 ± 0.04 nS, $n = 45$ neurons for treated; $P < 0.002$; Fig. 1*C*). PCs in VPA-treated rats therefore target more neurons, but the overall strength of the connection between each pair is reduced.

To find out whether the hyperconnectivity was unique to PCs, we examined the probability of activating one type of inhibitory interneurons by studying a disynaptic inhibitory connection between PCs (Silberberg and Markram 2007). We found a significant increase in the probability of disynaptic connections (67%; 0.33 ± 0.02, $n = 458$ pairs for control; 0.55 ± 0.02, $n = 420$ for treated; $P < 0.00001$; Fig. 1*D*). Although this measure does not reflect the involvement of the full spectrum of interneuron subtypes, it does show that the hyperconnectivity extends beyond the direct connections between PCs.

Reduced Cell Excitability

Hyperconnectivity of PCs may be correlated with changes in intrinsic neuronal properties. We therefore examined the electrical properties of the neurons. We found that PCs were markedly depressed in terms of their electrical excitability in slices from VPA-treated rats (Fig. 2*A*,*B*). The amount of current required to reach AP threshold was significantly increased (for layer 5 neurons: 400 ± 16 pA, $n = 51$ neurons for control, 444 ± 16 pA, $n = 31$ neurons for treated, $P < 0.05$; for layer 2/3 neurons: 145 ± 3 pA, $n = 89$ neurons for control, 168 ± 4 pA, $n = 100$ neurons for treated, $P < 0.0001$). The current–discharge slope was also significantly lowered (for layer 5 neurons: 0.029 ± 0.001

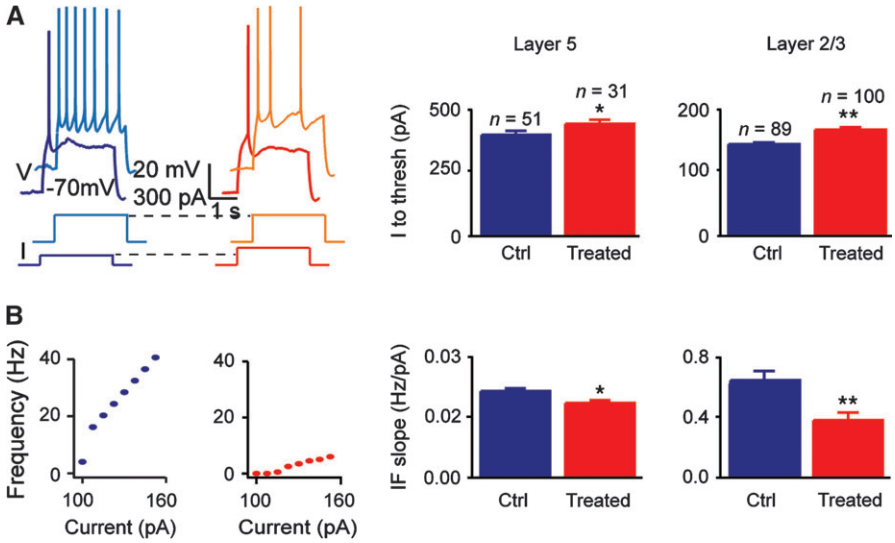

Figure 2. Hypoexcitability of PCs. (*A*) Example of currents injected and corresponding voltage measurements in layer 2/3 PCs from control (blue) and VPA-treated (red) rats. Mean of injected current to threshold for layer 5 and layer 2/3 PCs. (*B*) Example of the current–frequency (IF) curve for layer 2/3 PCs. Mean of IF slope (linear fit) for layer 5 and layer 2/3 PCs. Data show mean ± SEM (*$P < 0.05$; **$P < 0.01$; Student's *t*-test).

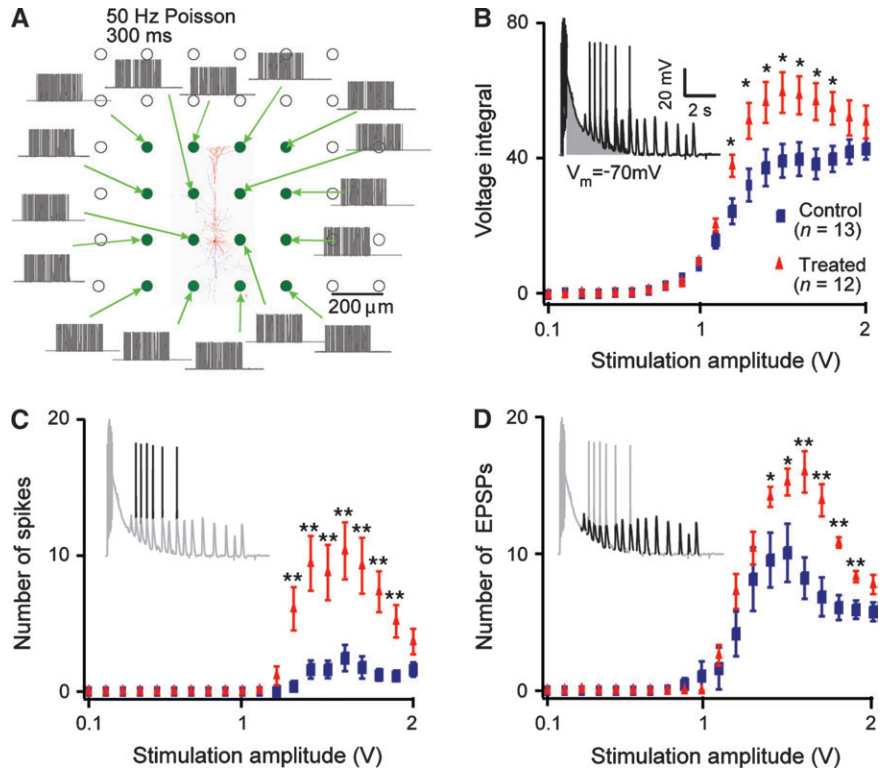

Figure 3. Hyperreactive network. (*A*) MEA stimulation with 16 electrodes (50-Hz Poisson train, 300 ms) in layer 5 thick-tufted PCs. (*B*) Integral of responses to MEA stimulation in current-clamped PCs as a function of stimulation amplitude. (*C*) Number of spikes elicited by the MEA stimulation as a function of the stimulation amplitude. (*D*) Number of excitatory postsynaptic potentials (EPSPs) elicited by the stimulation as a function of stimulation amplitude. The upper traces represent the response of a whole-cell patched layer 5 PC, with an emphasis on what is measured for each graph. Data show mean ± SEM (*$P < 0.05$; **$P < 0.01$; Student's *t*-test).

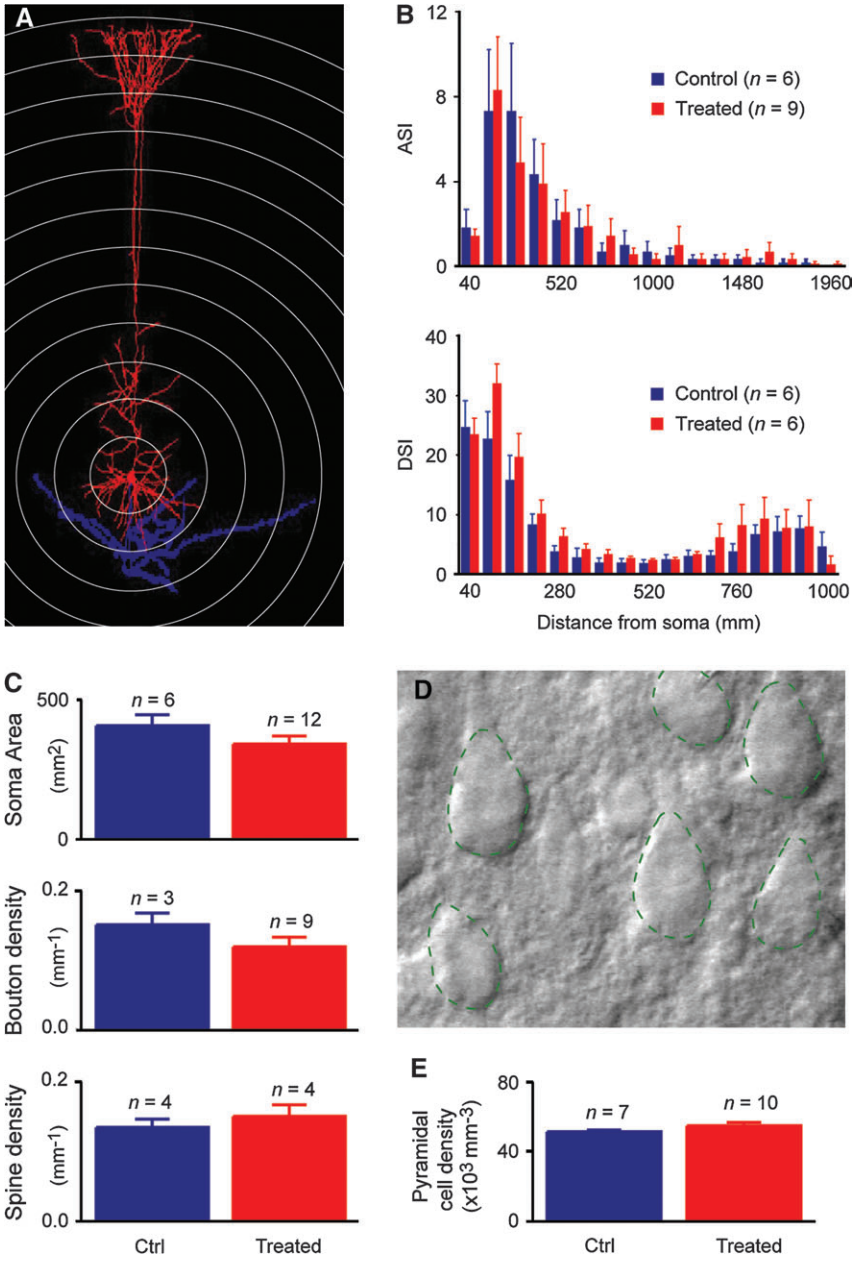

Figure 4. Anatomy of layer 5 PCs. (*A*) Example of Sholl analysis of a layer 5 thick-tufted PC. (*B*) Sholl analysis of the axonal (ASI) and dendritic (DSI) tree intersections. (*C*) Surface of the soma (406 ± 40 μm^2 for control, 340 ± 29 μm^2 for treated). Bouton density (0.15 ± 0.02/μm for control, 0.12 ± 0.01/μm for treated). Spine density (0.13 ± 0.01/μm for control, 0.15 ± 0.02/μm for treated). (*D*) Picture of layer 5 somatosensory cortex, as used for PC density counting. Thick-tufted PCs were recognized by their characteristic apical dendrite, soma shape, and size. The density was calculated in a volume of 180 × 180 × 30 μm. (*E*) Layer 5 PC density (52 ± 1 $\times 10^3/mm^3$ for control, 54 ± 2 $\times 10^3/mm^3$ for treated). Data show mean ± SEM; 2-sample Kolmogorov–Smirnoff test was used to compare ASI and DSI. All other means were compared with 2-sample Student's *t*-test.

Hz/pA, $n = 51$ neurons for control, 0.025 ± 0.001 Hz/pA, $n = 31$ neurons for treated, $P < 0.02$; for layer 2/3 neurons: 0.62 ± 0.08 Hz/pA, $n = 89$ neurons for control, 0.37 ± 0.05 Hz/pA, $n = 100$ neurons for treated, $P < 0.02$). However, the input resistance of PCs were not significantly different between control and treated rats (Supplementary Fig. 1). Other intrinsic properties, like AP amplitude, AP duration, or membrane time constant, were not different between control and treated PCs (data not shown).

Network Hyperreactivity

To explore in more detail the overall excitability at the network level, we examined the reactivity of the microcircuit to multisite extracellular electrical stimulation (Fig. 3). We measured the charge entering the recorded PCs following extracellular stimulation with increasing amplitude; this protocol provides a controlled measure of the microcircuit activity—involving intrinsic cell properties as well as extrinsic circuit properties—as reflected by synaptic input to the recorded neuron. The stimulus–response curve for thick-tufted layer 5 PCs of VPA-treated rats was significantly increased (Fig. 3*A*,*B*). The number of spikes (Fig. 3*C*) and the number of excitatory postsynaptic potentials (Fig. 3*D*) generated by this stimulation were also significantly higher. As the MEA stimulation is strong, the increase in the recorded responses could be due both to

changes in intrinsic cell properties and network properties. However, neither the study of intrinsic properties (Fig. 2) nor the study of calcium influx and handling (Rinaldi et al. 2007) do explain the higher responses observed with MEA stimulation in treated rats. The 3 measured parameters, that is, the charge entering the neurons, the number of APs, and the number of postsynaptic potentials evoked by stimulating the network with strong extracellular stimulation, therefore reflect the amount of reactivity of the network (Berger et al. 2006). Hence, these results indicate that the neocortical microcircuit of the VPA-treated rats is more reactive with respect to control. We conducted the same experiment in layer 2/3 PCs in voltage-clamp mode; the results confirmed the hyperreactive network observed in layer 5 PCs (Supplementary Fig. 2*C*), indicating that the hyperreactivity is not restricted to one neocortical layer.

We then isolated the excitatory and inhibitory synaptic current by voltage-clamping layer 2/3 PCs at the reversal potential for $GABA_A$ ($V_{hold} \approx -57$ mV) and AMPA receptors ($V_{hold} \approx +10$ mV), respectively. The stimulus–response curves for excitation and inhibition (Supplementary Fig. 2*C*) indicated that both were increased in the microcircuitry of the VPA-treated rats as compared with control rats. Interestingly, the ratio between excitation and inhibition remained constant for all stimulation amplitudes both in control and treated rats (data not shown), indicating that inhibitory pathways are faithfully activated to match the excitation in the microcircuit.

Reduced Number of Putative Contacts Per Connection

In order to determine if structural changes account for the hyperconnectivity in PCs, we examined whether there were any morphological alterations caused by the prenatal VPA treatment. Reconstructions of biocytin-stained PCs did not show any significant differences in the axonal or dendritic arbors (Fig. 4*A,B*) in the spine or bouton densities and in the size of PC somata (Fig. 4*C*). These anatomical findings suggest that gross structural differences in PCs alone do not account for the hyperconnectivity. In addition, the density of PCs did not differ (Fig. 4*D,E*), indicating that hyperconnectivity was not due to a smaller number of putative target neurons. To confirm this result, we also studied apoptosis to determine whether there was more cell loss in VPA-treated rats. TUNEL staining (see Materials and Methods) revealed a light pattern of neurodegeneration attributable to programmed cell death similar to apoptosis observed in controls (Supplementary Fig. 3), indicating that neurodegeneration and cell loss are not enhanced at this age in the VPA-treated rats.

We did, however, find that the average number of putative synaptic contacts localized within each connection was significantly lowered by 40% ($P < 0.05$): 3.3 ± 0.4 contacts ($n = 7$ connections) in slices from VPA-treated rats, compared with 5.0 ± 0.6 contacts ($n = 7$ connections) in layer 5 PC connections from control rats (Fig. 5).

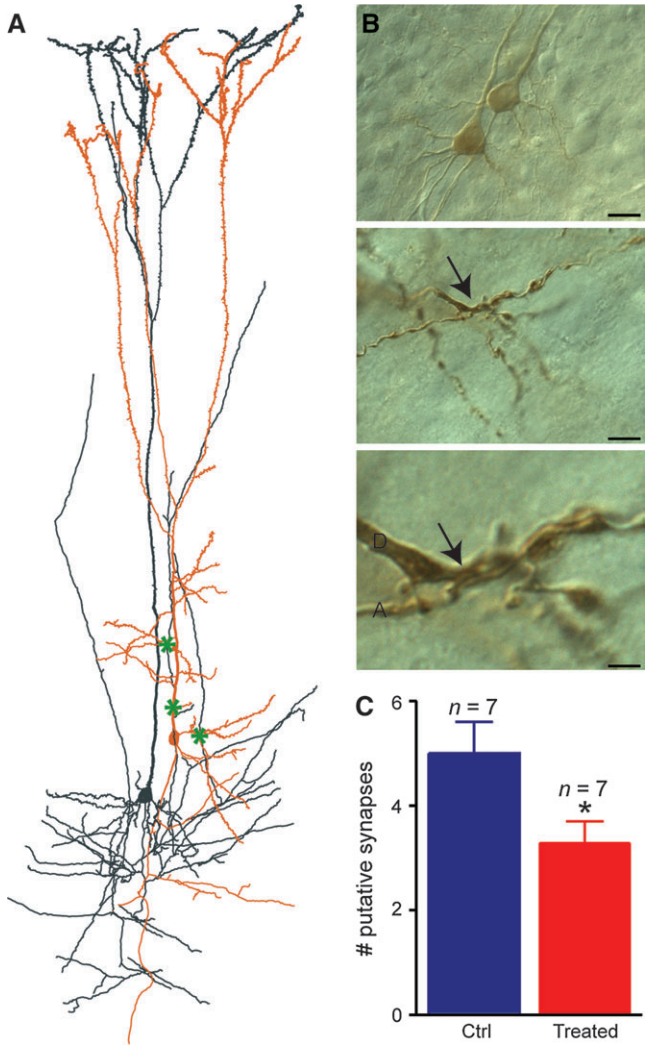

Figure 5. Decreased number of putative synaptic contacts in connected layer 5 PCs. (*A*) Example of the reconstruction of a connected pair of layer 5 PCs in the VPA-treated rats. The green asterisks represent the putative synapses. (*B*) Example of a pair of biocytin-stained cells and putative contact (arrow) between the axon of the presynaptic PC (*A*) and the dendrite of the postsynaptic PC (*D*). The scale bars represent 20, 10, and 2 μm. (*C*) Average number of putative contacts per connection between layer 5 PCs (5.0 ± 0.6 contacts for control, 3.3 ± 0.4 contacts for treated). Data show mean ± SEM (*$P < 0.05$; Student's *t*-test).

Discussion

We examined alterations in the basic properties of neocortical microcircuit in rats prenatally exposed to VPA. We report that a single prenatal injection of VPA causes a significant increase in the connection probability of layer 5 PCs, although the strength of the connections diminishes. PCs are also less excitable in treated as compared with control rats, as demonstrated with the significantly smaller slope of the current–frequency relationship. Using MEA stimulation, we further showed that the somatosensory cortex of treated rats generates greater responses to network stimulation. Finally, morphological reconstruction of connected pairs of PCs revealed a significant smaller number of putative synaptic contacts in slices of VPA-treated rats.

Homeostasis following Prenatal VPA Exposure

It is possible that the altered microcircuit properties described in this study are all independent consequences of the VPA insult. However, it might also be that the early VPA insult only causes part of these alterations and that the others are compensatory mechanisms. The compensatory mechanisms would allow the system to sustain stability and avoid over-excitation or quiescence. Such normalization mechanisms, counterbalancing the effect of a primary alteration, are known phenomena of the brain. Indeed, homeostatic processes have

already been described and their importance put forward in the literature of brain research (Buzsaki et al. 2002; Turrigiano and Nelson 2004), although many questions remain about their mechanisms and functions. A crucial step in understanding the alterations observed in the VPA rat model is to find out which alterations are direct consequences of the VPA insult and which are normalizing mechanisms counterbalancing the primary alterations. It is possible that the network ends up in a hyperconnected state following an attempt to compensate for the decreased PC excitability, but we rather speculate that the hypoexcitability is a compensatory mechanism because it seems less likely that hyperconnectivity would overcompensate to render the network more reactive. The decreased excitability of PCs and the reduced synaptic strength in PC connections may therefore reflect homeostatic processes following the stimulus-induced recruitment of too many neurons due to a hyperconnected network.

Diminished Selectivity of Synapse Formation and Elimination

The average number of putative synaptic contacts was demonstrated to be significantly diminished in connections from treated rats. This result suggests that the underlying mechanism for the observed hyperconnectivity is due to less selective synapse formation and elimination, the consequences being an increase in the number of target neurons for a given PC, accompanied by a reduction in the number of synaptic contacts formed between connected PCs. The reason for this abnormal synaptic process is unknown. Hyperconnectivity does not seem to occur due to a straightforward hypertrophy of the number of synapses because such deficit would increase the number of connections between neurons as well as the number of synapses within each connection. It could be that pruning is abnormal, acting in the whole microcircuitry without considering the role of the synapses as part of a useful or unnecessary connection; it could also be that the circuit is trapped in a less developed stage. Further work is needed to resolve and provide mechanistic insights into these differences between control and VPA-treated rats at an earlier developmental stage.

Increased Local Cortical Wiring and Autism

Hyperconnectivity was found to be a highly localized phenomenon affecting close neighboring neurons (<50 μm). Whether the enhanced local connectivity occurs at the expense of longer range input connections involved in attention or sensory integration has not yet been studied. Functional magnetic resonance imaging studies in humans do show impaired long-range functional connectivity in autism (Castelli et al. 2002; Just et al. 2004), and stronger local processing has been speculated (Casanova et al. 2002; Rubenstein and Merzenich 2003; Belmonte et al. 2004; Courchesne et al. 2005). This study could be the first proof for the hypothesis that local cortical wiring may be increased in autism.

We hypothesize that increased local PC connectivity could render cortical microcircuits more sensitive to external stimulation and trigger exaggerated activity. Once activated, local circuit activity may be more autonomous, impairing the ability of distal brain regions to effectively orchestrate neocortical activity in the functional modules of the neocortex. These impairments may therefore account for some of the core symptoms in children prenatally exposed to VPA.

Supplementary Material

Supplementary material can be found at: http://www.cercor.oxfordjournals.org/.

Funding

National Alliance for Autism Research; European Commission for the EUSynapse project (LSHM-CT-2005-019055); HFSP long term fellowship for G.S. (LT00330/2005-L).

Notes

We thank Phil Goodman, Thomas Berger, Brandi Mattson, Jean-Vincent Le Bé, Michele Pignatelli, Pavel Sekatski, Thomas Brionne, and Anirudh Gupta for their help. *Conflict of Interest*: None declared.

Address correspondence to email: henry.markram@epfl.ch.

References

Arndt TL, Stodgell CJ, Rodier PM. 2005. The teratology of autism. Int J Dev Neurosci. 23:189–199.

Belmonte MK, Allen G, Beckel-Mitchener A, Boulanger LM, Carper RA, Webb SJ. 2004. Autism and abnormal development of brain connectivity. J Neurosci. 24:9228–9231.

Berger T, Luscher HR, Giugliano M. 2006. Transient rhythmic network activity in the somatosensory cortex evoked by distributed input in vitro. Neuroscience. 140:1401–1413.

Binkerd PE, Rowland JM, Nau H, Hendrickx AG. 1988. Evaluation of valproic acid (VPA) developmental toxicity and pharmacokinetics in Sprague-Dawley rats. Fundam Appl Toxicol. 11:485–493.

Borg-Graham L, Monier C, Fregnac Y. 1996. Voltage-clamp measurement of visually-evoked conductances with whole-cell patch recordings in primary visual cortex. J Physiol Paris. 90:185–188.

Brionne TC, Tesseur I, Masliah E, Wyss-Coray T. 2003. Loss of TGF-beta 1 leads to increased neuronal cell death and microgliosis in mouse brain. Neuron. 40:1133–1145.

Buxhoeveden DP, Casanova MF. 2002. The minicolumn hypothesis in neuroscience. Brain. 125:935–951.

Buzsaki G, Csicsvari J, Dragoi G, Harris K, Henze D, Hirase H. 2002. Homeostatic maintenance of neuronal excitability by burst discharges in vivo. Cereb Cortex. 12:893–899.

Casanova MF, Buxhoeveden DP, Switala AE, Roy E. 2002. Minicolumnar pathology in autism. Neurology. 58:428–432.

Castelli F, Frith C, Happe F, Frith U. 2002. Autism, Asperger syndrome and brain mechanisms for the attribution of mental states to animated shapes. Brain. 125:1839–1849.

Christianson AL, Chesler N, Kromberg JG. 1994. Fetal valproate syndrome: clinical and neuro-developmental features in two sibling pairs. Dev Med Child Neurol. 36:361–369.

Courchesne E, Redcay E, Morgan JT, Kennedy DP. 2005. Autism at the beginning: microstructural and growth abnormalities underlying the cognitive and behavioral phenotype of autism. Dev Psychopathol. 17:577–597.

Ingram JL, Peckham SM, Tisdale B, Rodier PM. 2000. Prenatal exposure of rats to valproic acid reproduces the cerebellar anomalies associated with autism. Neurotoxicol Teratol. 22:319–324.

Just MA, Cherkassky VL, Keller TA, Minshew NJ. 2004. Cortical activation and synchronization during sentence comprehension in high-functioning autism: evidence of underconnectivity. Brain. 127:1811–1821.

Le Be JV, Silberberg G, Wang Y, Markram H. 2006. Morphological, electrophysiological, and synaptic properties of corticocallosal pyramidal cells in the neonatal rat neocortex. Cereb Cortex. Advance Access published on November 23, 2006; doi:10.1093/cercor/bhl127.

Markram H, Lubke J, Frotscher M, Roth A, Sakmann B. 1997. Physiology and anatomy of synaptic connections between thick tufted pyramidal neurones in the developing rat neocortex. J Physiol. 500(Pt 2):409–440.

Markram H, Wang Y, Tsodyks M. 1998. Differential signaling via the same axon of neocortical pyramidal neurons. Proc Natl Acad Sci USA. 95:5323–5328.

Markram K, Rinaldi T, La Mendola D, Sandi C, Markram H. Forthcoming 2007. Abnormal fear conditioning and amygdala processing in an animal model of autism. Neuropsychopharmacology. advance online publication, 16 May 2007. doi: 10.1038/sj.npp.1301453.

Moore SJ, Turnpenny P, Quinn A, Glover S, Lloyd DJ, Montgomery T, Dean JC. 2000. A clinical study of 57 children with fetal anticonvulsant syndromes. J Med Genet. 37:489–497.

Rasalam AD, Hailey H, Williams JH, Moore SJ, Turnpenny PD, Lloyd DJ, Dean JC. 2005. Characteristics of fetal anticonvulsant syndrome associated autistic disorder. Dev Med Child Neurol. 47:551–555.

Rinaldi T, Kulangara K, Antoniello K, Markram H. Forthcoming 2007. Elevated NMDA receptor levels and enhanced postsynaptic long term potentiation induced by prenatal exposure to valproic acid. Proc Natl Acad Sci USA. In Press.

Rodier PM, Ingram JL, Tisdale B, Croog VJ. 1997. Linking etiologies in humans and animal models: studies of autism. Reprod Toxicol. 11:417–422.

Rubenstein JL, Merzenich MM. 2003. Model of autism: increased ratio of excitation/inhibition in key neural systems. Genes Brain Behav. 2:255–267.

Schneider T, Przewlocki R. 2005. Behavioral alterations in rats prenatally exposed to valproic acid: animal model of autism. Neuropsychopharmacology. 30:80–89.

Silberberg G, Markram H. 2007. Disynaptic inhibition between neocortical pyramidal cells mediated by Martinotti cells. Neuron. 53:735–746.

Sobaniec-Lotowska ME. 2001. Ultrastructure of Purkinje cell perikarya and their dendritic processes in the rat cerebellar cortex in experimental encephalopathy induced by chronic application of valproate. Int J Exp Pathol. 82:337–348.

Tsodyks MV, Markram H. 1997. The neural code between neocortical pyramidal neurons depends on neurotransmitter release probability. Proc Natl Acad Sci USA. 94:719–723.

Turrigiano GG, Nelson SB. 2004. Homeostatic plasticity in the developing nervous system. Nat Rev Neurosci. 5:97–107.

Williams G, King J, Cunningham M, Stephan M, Kerr B, Hersh JH. 2001. Fetal valproate syndrome and autism: additional evidence of an association. Dev Med Child Neurol. 43:202–206.

Williams PG, Hersh JH. 1997. A male with fetal valproate syndrome and autism. Dev Med Child Neurol. 39:632–634.